Unidirectional and controllable higher-order diffraction by a Rydberg electromagnetically induced grating

Dandan Ma,[1] Dongmin Yu,[1] Xing-Dong Zhao,[2] and Jing Qian[1,*]

[1]*State Key Laboratory of Precision Spectroscopy, Department of Physics, School of Physics and Material Science, East China Normal University, Shanghai 200062, China*

[2]*College of Physics and Materials Science, Henan Normal University, Xinxiang 453007, China*

(Received 11 November 2018; published 13 March 2019)

A method for diffracting the weak probe beam into unidirectional and higher-order directions is proposed via a Rydberg electromagnetically induced grating, providing a way for the implementations of quantum devices with cold Rydberg atoms. The proposed scheme utilizes a suitable position-dependent adjustment to the two-photon detuning besides the modulation of the standing-wave coupling field, producing an in-phase modulation which can change the parity of the dispersion. We observe that when the modulation amplitude is appropriate, a perfect unidirectional diffraction grating can be realized. In addition, due to the mutual effect between the van der Waals (vdW) interaction and the atom-field interaction length that deeply improves the dispersion of the medium, the probe energy can be counterintuitively transferred into higher-order diffractions as increasing the vdW interaction, leading to the realization of a controllable higher-order diffraction grating via a strong blockade.

DOI: 10.1103/PhysRevA.99.033826

I. INTRODUCTION

In the field of quantum simulation, designing controllable quantum devices such as a quantum gate, a quantum annealer based on a cold atomic medium, has achieved significant progress, mainly because of long coherence times and flexible manipulation possessed by an atom-field interacting system at a low temperature [1]. An ultracold neutral atomic source can be used to realize a robust quantum simulator taking advantage of its internal hyperfine levels serving as qubits [2,3], providing further operations for multiparticle entanglement [4] and a fast quantum gate [5]. Undoubtedly, a highly excited Rydberg atom, as one of the neutral atoms, has manifested as an attractive candidate to maintain the coherence and for the realization of new quantum devices in the field of quantum simulation, applying, for example, to the quantum simulator in a spin model by the strong many-body interactions [6] and the controlled high-fidelity entanglement with a reduced-phase-noise laser [7].

In parallel, electromagnetically induced transparency (EIT) [8] plays a significant role in studies of optical devices in an atomic medium, offering great advances for nonlinear quantum optics [9]. Electromagnetically induced transparency essentially utilizes quantum interference of double optical transitions to make the absorption of the weak probe field vanish, resulting in an EIT window to enhance the probe transmission even in the case of resonant probe detuning. In a Rydberg system, by coupling the probe transition to a Rydberg state via EIT, the strong van der Waals (vdW) interactions between two Rydberg states can be translated into sizable interactions between photons, resulting in cooperative optical nonlinearity [10]. In addition, EIT has been applied to store the gate photon as a Rydberg excitation, realizing various quantum devices such as single-photon switches [11,12] or transistors [13,14].

It is remarkable that, in a Rydberg EIT system, when the strong-coupling field is replaced by a standing-wave (SW) field, implementing a spatial periodic modulation for the absorption (amplitude) and dispersion (phase) of medium, the traveling-wave (TW) probe field can be diffracted into higher-order directions. This is called a Rydberg electromagnetically induced grating (EIG), serving as another member in the family of Rydberg quantum devices. A normal atomic EIG, first proposed by Ling [15] and observed by Mitsunaga and Imoto in sodium atoms [16], has been widely explored (see, e.g., [17–21]). Other schemes created diffraction gratings based on the modulation of Raman gain without EIT tools [22,23]. Here differing from the normal ones, the proposed Rydberg EIG with the uppermost level replaced by a Rydberg level is significantly influenced by the vdW interaction. Intuitively, the diffraction intensity will exponentially decrease with the increase of vdW interaction due to the breakup of EIT condition, representing no notable results [24].

Motivated by a recent work [25] where authors exploited an asymmetric EIG with parity-time symmetry to the coupling field breaking the parity of absorption and realized the diffraction of the probe field into either negative or positive angles, we propose an approach for achieving an exotic Rydberg EIG with perfect unidirectional and higher-order diffraction. The key lies in introducing a suitable periodic modulation to the two-photon detuning in order to break the parity of dispersion, resulting in a position-dependent modulation to the energy of the Rydberg level aside from the vdW shift. As a result, we

*jqian1982@gmail.com

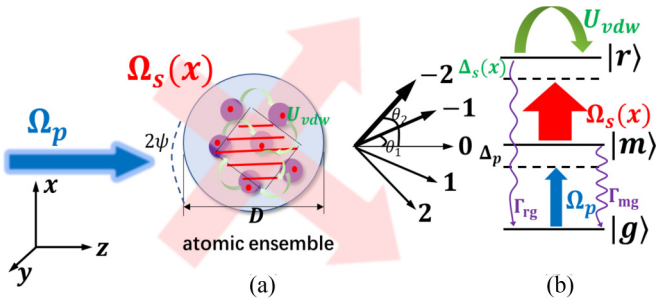

FIG. 1. (a) Schematic representation of a normal Rydberg EIG. A single atomic ensemble with cascade three-level atoms is coupled by a strong SW coupling field and a weak TW probe field. When the incident probe field normally propagates through such an ensemble it can be diffracted into high-order diffractions due to the phase and amplitude modulations exerted by the SW coupling field. (b) Atomic energy levels. The vdW-type interaction $U_{\rm vdW}$ presents if atoms are simultaneously excited to the Rydberg state $|r\rangle$ due to the imperfection of full blockade. Relevant parameters are described in the text.

observe a perfect unidirectional diffraction with the peak nth-order diffraction intensities satisfying $I_p^{\rm pk}(\theta_0) > I_p^{\rm pk}(\theta_{-1}) > I_p^{\rm pk}(\theta_{-2}) > I_p^{\rm pk}(\theta_{-3})$, under the condition of an appropriate modulation amplitude of detuning. More interestingly, the diffraction intensity represents a strong oscillatory behavior and is found to be transferred into higher-order diffractions by increasing the strength of the vdW interaction, leading to a controllable enhanced higher-order diffraction grating via an optimal control for the vdW interaction. Our scheme is of significant interest to scientists for the design of various quantum devices such as a large-angle optical splitter with Rydberg atoms.

II. ATOM-FIELD INTERACTION MODEL

We consider that a single ensemble with N atoms has a cascading three-level structure (see Fig. 1), driven by a weak TW probe field and a strong SW coupling field, whose Rabi frequencies are denoted by Ω_p and $\Omega_s(x)$ $[=\Omega_{s0}\sin(\frac{\pi x}{\Lambda_{sx}})]$, respectively. Here Ω_p and Ω_{s0} are the peak amplitudes and $\Lambda_{sx} = \lambda_s/\sin\psi$ is the SW spatial period on the x axis with λ_s the coupling wavelength and ψ the azimuth. The energy level of each atom is composed of a Rydberg state $|r\rangle$, an intermediate excited state $|m\rangle$, and a ground state $|g\rangle$, respectively, making $|g\rangle \to |m\rangle$ and $|m\rangle \to |r\rangle$ transitions. Note that, in a normal EIG, the strong SW field $\Omega_s(x)$ will exert a spatial periodic change on the refractive index of the atomic medium, leading to a far-field Fraunhofer diffraction of the weak probe field as it propagates through the medium [15], and it becomes a Rydberg EIG when the uppermost level is a Rydberg state [26].

Actually, the typical timescales for Rydberg experiments is maximally on the order of the Rydberg lifetime (on the order of microseconds) during which the ultracold atoms move only small distances relative to their separations, leading to a negligence of the atomic motion in the frozen-gas environment [27–29]. Here we assume that the interatomic interaction between two Rydberg atoms is of vdW type [30]; therefore the Hamiltonian in the frame of the rotating-wave approximation can be written as $\mathcal{H} = \mathcal{H}_a + \mathcal{U}_{af} + \mathcal{U}_{\rm vdW}$, which consists of an unperturbed atomic part $\mathcal{H}_a = -\hbar\sum_j^N[\Delta_p\sigma_{mm}^j + \Delta_s\sigma_{rr}^j]$, an atom-field coupling part $\mathcal{U}_{af} = -\hbar\sum_j^N[\Omega_p\sigma_{mg}^j + \Omega_s(x)\sigma_{rm}^j + {\rm H.c.}]$, and an interaction part $\mathcal{U}_{\rm vdW} = \hbar\sum_{i<j}^N\frac{C_6}{|r_i-r_j|^6}\sigma_{rr}^i\sigma_{rr}^j$. Here the transition operator is $\sigma_{\alpha\beta}^j = |\alpha\rangle\langle\beta|_j$ $(\alpha \neq \beta)$, the projection operator is $\sigma_{\alpha\alpha}^j = |\alpha\rangle\langle\alpha|_j$, $\Delta_{p\,(s)}$ is the one-photon (two-photon) detuning, C_6 is the vdW coefficient, and $|r_i - r_j|$ is the interatomic distance. In addition, $N = \rho V$ defines the number of atoms, with ρ the atomic density and V the volume. Note that $1/\rho = 4\pi R^3/3$ represents the occupied space of a single atom, with R the average interatomic spacing. For the jth atom, the interaction part can be replaced by $\mathcal{U}_{\rm vdW} = \hbar\sum_j^N\sigma_{rr}^j\sum_{i\neq j}\frac{C_6}{|r_i-r_j|^6}\sigma_{rr}^i$ under the mean-field treatment [31], by which the many-body interacting system is replaced by a model of one atom j affected by the accumulated level shifts from other nearby exciting atoms. Note that the atom-atom correlations are neglected in this approximation.

To this end, the time evolution for $\sigma_{\alpha\beta}^j$ can be governed by the motional equations

$$\dot\sigma_{gg}^j = i\Omega_p\sigma_{gm}^j - i\Omega_p^*\sigma_{mg}^j + 2\gamma_{gm}\sigma_{mm}^j, \tag{1}$$

$$\dot\sigma_{rr}^j = i\Omega_s\sigma_{mr}^j - i\Omega_s^*\sigma_{rm}^j, \tag{2}$$

$$\dot\sigma_{gm}^j = (i\Delta_p - \gamma_{gm})\sigma_{gm}^j + i\Omega_p^*(\sigma_{gg}^j - \sigma_{mm}^j) + i\Omega_s\sigma_{gr}^j, \tag{3}$$

$$\dot\sigma_{gr}^j = i(\Delta_s - s)\sigma_{gr}^j + i\Omega_s^*\sigma_{gm}^j - i\Omega_p^*\sigma_{mr}^j, \tag{4}$$

$$\dot\sigma_{mr}^j = [i((\Delta_s - s) - \Delta_p) - \gamma_{gm}]\sigma_{mr}^j + i\Omega_s^*(\sigma_{mm}^j - \sigma_{rr}^j) - i\Omega_p\sigma_{gr}^j, \tag{5}$$

where γ_{gm} is the dephasing rate of the $|g\rangle \to |m\rangle$ transition and $\Gamma_{m(r)}$ is the spontaneous decay rate of $|m(r)\rangle$. In deriving Eqs. (1)–(5) we have used the relations $\Gamma_m = 2\gamma_{gm}$ and $\gamma_{mr} = \gamma_{gm}$ by considering $\gamma_{\alpha\beta} = (\Gamma_\alpha + \Gamma_\beta)/2$ $[\alpha, \beta \in (g, m, r)]$ and $\Gamma_m \gg \Gamma_r$ [32,33]. In addition, $s = \sum_{i\neq j}\frac{C_6}{|r_i-r_j|^6}\sigma_{rr}^i$ characterizes the interaction-induced energy shifts to the state $|r_j\rangle$ caused by other exciting atoms within the ensemble. Typically these atoms exist beyond the blockade radius.

We further replace the sum in s with a spatial integral standing for all interactions of exciting atoms. In fact, only one atom is excited within a blockade radius R_b and the separation r between two exciting atoms meets $r > R_b$, so it is reasonable to introduce a short-range cutoff to the spatial integral at R_b [34,35],

$$s \approx \int_{R_b}^{\infty}\frac{C_6}{r^6}\sigma_{rr}\rho 4\pi r^2 dr = \frac{4\pi C_6}{3R_b^3}\rho\sigma_{rr}, \tag{6}$$

where $\rho\sigma_{rr}$ represents the atomic exciting density in the ensemble. First, the steady-state solutions σ_{rr}, σ_{gm}^R, and σ_{gm}^I

can be formally expressed, by assuming $\dot{\sigma}^{j}_{\alpha\beta}=0$, as

$$\sigma_{rr}=\frac{\Omega_p^2\left[\Omega_p^2+\Omega_s(x)^2\right]}{\left[\Omega_p^2+\Omega_s(x)^2\right]^2+2\Delta_p(\Delta_s-s)\Omega_s(x)^2+(\Delta_s-s)^2\left(\gamma_{gm}^2+\Delta_p^2+2\Omega_p^2\right)}, \tag{7}$$

$$\sigma^{I}_{gm}=\frac{\gamma_{gm}(\Delta_s-s)^2\Omega_p}{\left[\Omega_p^2+\Omega_s(x)^2\right]^2+2\Delta_p(\Delta_s-s)\Omega_s(x)^2+(\Delta_s-s)^2\left(\gamma_{gm}^2+\Delta_p^2+2\Omega_p^2\right)}, \tag{8}$$

$$\sigma^{R}_{gm}=\frac{(\Delta_s-s)[\Omega_s(x)^2-\Delta_p(\Delta_s-s)]\Omega_p}{\left[\Omega_p^2+\Omega_s(x)^2\right]^2+2\Delta_p(\Delta_s-s)\Omega_s(x)^2+(\Delta_s-s)^2\left(\gamma_{gm}^2+\Delta_p^2+2\Omega_p^2\right)}, \tag{9}$$

with s a relevant parameter with respect to σ_{rr} as in Eq. (6). The solution of σ_{rr} is nonlinear and complicated. Consequently, it is hard to estimate s exactly.

Note that the formal solution σ_{rr} is a Lorentzian-like function with respect to Δ_s by considering $s=0$ in Eq. (7) (only one exciting atom) and $\Delta_p \ll \gamma_{gm}$, giving rise to the half-linewidth of single-atom Rydberg probability: $\omega=(\Omega_p^2+\Omega_s^2)/\sqrt{\gamma_{gm}^2+\Delta_p^2+2\Omega_p^2}$. To quantitatively estimate s, we find that the single-atom blockade radius can be roughly given by $R_b=(C_6/\omega)^{1/6}$ [36]. With definitions of R and R_b, we can finally arrive at a reduced form of the approximated interaction s, which is [37]

$$s=\frac{\omega}{\xi}\sigma_{rr}\approx\frac{\Omega_p^2}{\xi\sqrt{\gamma_{gm}^2+\Delta_p^2+2\Omega_p^2}}, \tag{10}$$

where we used approximated σ_{rr} obtained by the formal solution under the assumption of $s=0$ for single-atom excitation and $\Delta_p \ll \gamma_{gm}$ and $\Delta_s<\Omega_s$. The coefficient $\xi=(R/R_b)^3$ is treated as an adjustable parameter controlled by the atomic density ρ, which stands for the strength of simultaneous excitation of nearby atoms to the Rydberg state. Here $\xi>1$ means the blockade is imperfect. Substituting Eq. (10) into Eqs. (7)–(9) finally gives rise to the analytical expressions for the steady solutions σ_{rr}, σ^{I}_{gm}, and σ^{R}_{gm}. We note that the parameters σ^{R}_{gm} and σ^{I}_{gm} can directly lead to a position-dependent polarization to the probe field with the probe susceptibility given by

$$\chi_p(x)=\eta\left(\sigma^{R}_{gm}+i\sigma^{I}_{gm}\right), \tag{11}$$

where $\eta=2\rho\mu_{gm}^2/\hbar\epsilon_0\Omega_p$ [20]. Here the real part $\eta\sigma^{R}_{gm}$ of susceptibility stands for the response of dispersion of the medium and the imaginary part $\eta\sigma^{I}_{gm}$ for the medium absorption response.

III. POSITION-DEPENDENT TWO-PHOTON DETUNING

For an atomic medium modulated by the strong SW field along the x axis, the transmission function for the probe field can be solved from the propagation equation, given by

$$T(x)=e^{-\alpha(x)D+i\beta(x)D}, \tag{12}$$

where $\alpha(x)=(2\pi\eta/\lambda_p)\sigma^{I}_{gm}$ and $\beta(x)=(2\pi\eta/\lambda_p)\sigma^{R}_{gm}$ represent the amplitude and phase modulations, respectively. The atom-field interaction length $D=\zeta z_0$, with optical depth ζ in units of $z_0=\frac{\lambda_p}{2\pi\xi\eta}$ (λ_p is the probe wavelength), characterizes the length of the atom-field interaction along the z axis. By carrying out the Fourier transformation of $T(x)$ we can obtain the nth-order diffraction intensity of the probe field, given by

$$I_p(\theta_n)=|E_p(\theta_n)|^2\frac{\sin^2[M\pi\Lambda_{sx}\sin(\theta_n)/\lambda_p]}{M^2\sin^2[\pi\Lambda_{sx}\sin(\theta_n)/\lambda_p]}, \tag{13}$$

where the intensity in a single period is

$$E_p(\theta_n)=\int_{-\Lambda_{sx}/2}^{+\Lambda_{sx}/2}T(x)e^{-i2\pi nx}dx, \tag{14}$$

$n=\Lambda_{sx}\sin\theta_n/\lambda_p$ is the diffraction order, and M is the number of grating periods defined by the ratio between the beam width of Ω_p and the grating periodic number Λ_{sx}. The overall output $I_{\rm out}=\sum_n I_p^{\rm pk}(\theta_n)$ ($n=0,\pm1,\pm2,\ldots$) is defined by all maximal nth-order diffraction intensities $I_p^{\rm pk}(\theta_n)$.

It is well known that a normal Rydberg EIG with symmetric diffraction intensities can be created, stemming from a spatial modulation by the strong-coupling field $\Omega_s(x)$, to modify the dispersion $\eta\sigma^{R}_{gm}$ and absorption $\eta\sigma^{I}_{gm}$ of the medium [24]. For η constant we will omit it and treat σ^{R}_{gm} (σ^{I}_{gm}) as dispersion (absorption) in the following discussion. As a result, σ^{R}_{gm} and σ^{I}_{gm} show spatially symmetric even functions, yielding symmetric diffraction patterns [see, e.g., Fig. 3(a iii)]. Observing exotic unidirectional diffraction (UD) requires the breakup of this symmetry; for that purpose, we introduce a suitable position-dependent adjustment to the two-photon detuning $\Delta_s(x)$, which can change the parity of the dispersion σ^{R}_{gm} [Eq. (9)]. Similar spatial modulation to the light shift was considered in a lattice system manipulated by tuning the orientation of laser beams [38].

Here, to realize easy experimental control, we give an in-phase spatial modulation to $\Delta_s(x)$, similar as $\Omega_s(x)$, with δ the modulation amplitude and Δ_{s0} the constant detuning,

$$\Delta_s(x)=\Delta_{s0}+\delta\sin(\pi x/\Lambda_{sx}), \tag{15}$$

which can be realized by the ac Stark effect to induce a periodic change of energy shift of the state $|r\rangle$. In experiment, one can use extra spatially modulated strong lasers for that purpose [39]. The position-dependent two-photon detuning $\Delta_s(x)$ accompanying $\Omega_s(x)$ will lead to an anomalous change for the dispersion function $\sigma^{R}_{gm}(x)$, making it noneven. It is expected that, in the case of $\delta=0$ and $\Delta_s=\Delta_{s0}$, one creates a normal Rydberg EIG because σ^{R}_{gm} is exactly an even function.

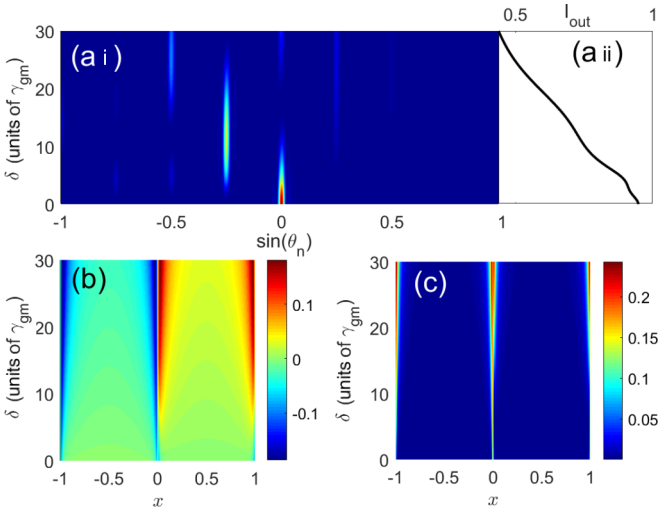

FIG. 2. (a i) Diffraction intensity $I_p(\theta_n)$ versus the modulation amplitude δ and the diffraction angle $\sin\theta_n$ for $\Delta_{s0} = 0$. As δ increases, the diffraction intensity disperses into higher-order directions. (a ii) Overall output $I_{\rm out}$ versus δ. The values of (b) dispersion σ^R_{gm} and (c) absorption σ^I_{gm} are shown versus δ and x. Other specific parameters are $\Omega_p = 0.5\gamma_{gm}$, $\Omega_{s0} = 22.5\gamma_{gm}$, $\Delta_p = 0$, $M = 10$, $\zeta = 200$, and $\xi = 3.0$.

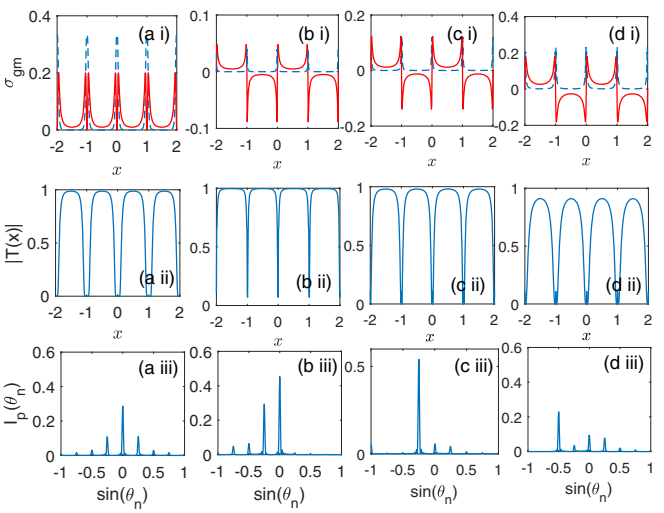

FIG. 3. Plots of dispersion σ^R_{gm} (red solid line), absorption σ^I_{gm} (blue dashed line), transmission $|T(x)|$, and diffraction pattern $I_p(\theta_n)$ for (a i)–(a iii) $\Delta_{s0}/\gamma_{gm} = 10$ and $\delta = 0$, (b i)–(b iii) $\Delta_{s0} = 0$ and $\delta/\gamma_{gm} = 5$, (c i)–(c iii) $\Delta_{s0} = 0$ and $\delta/\gamma_{gm} = 12.5$, and (d i)–(d iii) $\Delta_{s0} = 0$ and $\delta/\gamma_{gm} = 27$ respectively.

The resulting probe diffraction is expected to be diffracted uniformly into both positive and negative angles. However, in the case of $\delta \neq 0$, $\Delta_s(x)$ will cause the key diffraction player, dispersion σ^R_{gm}, to be out of phase and an exotic UD may be observed.

IV. NUMERICAL RESULTS AND DISCUSSION

A. Unidirectional diffraction

To see the effect of the modulation from the detuning, we first plot the probe diffraction intensity $I_p(\theta_n)$ versus the modulation amplitude δ and the angle $\sin(\theta_n)$ in Fig. 2(a i). The overall output intensity $I_{\rm out}$ versus δ is shown in Fig. 2(a ii). In general, if $\delta \neq 0$ the diffraction is basically asymmetric and disperses into higher-order diffractions with the increase of δ, accompanied by a slow decrease for the overall output $I_{\rm out}$ due to the absorption effect. A special case is for $\delta = 0$, when the diffraction intensity totally gathers into the zeroth-order direction where only the SW coupling field plays a role, and it further disperses for $\delta \neq 0$ owing to the growth of dispersion affected by the periodic modulation from the two-photon detuning, giving rise to a UD grating. The underlying physics comes from the breakup of parity of the dispersion function [see Eq. (9)], that is, $\sigma^R_{gm} \propto [\Delta_s(x) - s]\Omega_s(x)^2$. When $\Delta_s(x) = \Delta_{s0}$, σ^R_{gm} is even; otherwise it is modulated to be noneven with respect to $x = 0$.

Figures 2(b) and 2(c) show the variations of dispersion and absorption functions versus δ and x. Clearly, σ^R_{gm} is modulated to contain positive and negative values as δ increases while σ^I_{gm} continues to increase, resulting in a continuous reduction in $I_{\rm out}$. In other words, for a larger δ, both dispersion σ^R_{gm} and absorption σ^I_{gm} are improved, however only the parity of dispersion is significantly changed by the modulation.

Specific results for $\delta/\gamma_{gm} = (0, 5.0, 12.5, 27)$ are presented in Fig. 3, where the patterns of dispersion, absorption, transmission, and diffraction intensities are respectively shown. As expected, for $\delta = 0$ and $\Delta_{s0}/\gamma_{gm} = 10$ [Fig. 3(a iii)], the diffraction intensity $I_p(\theta_n)$ represents a perfect symmetric distribution with positive and negative diffraction angles owing to the even functions of σ^R_{gm} and σ^I_{gm}, which are solely modulated by the SW coupling field. As δ is increased to $5.0\gamma_{gm}$, the diffraction intensity becomes anomalously unidirectional and is distributed only in the range of negative angles. It is remarkable that this diffraction direction can be manipulated by changing the sign of modulation amplitude δ easily. A further increase of δ leads to the primary diffraction order transfers to negative first-order [Fig. 3(c iii)] and second-order [Fig. 3(d iii)] directions because of the growth of dispersion σ^R_{gm}. Meanwhile, the increase of absorption induces a slight reduction of the transmission as well as the overall output.

To search for the optimal conditions of a perfect UD [e.g., Fig. 3(b iii)], focusing on the competition between $\Delta_s(x)$ and $\Omega_s(x)$, we study the diffraction intensity $I_p(\theta_n)$ versus the variation of Ω_{s0} and $\sin(\theta_n)$ while keeping δ and Ω_p constant. It can be clearly seen that $I_p(\theta_n)$ [Fig. 4(a i)] presents the opposite behavior with respect to that in Fig. 2(a i), i.e., the diffraction intensity gathers in the zeroth-order direction with increasing Ω_{s0}. The resulting overall output $I_{\rm out}$ keeps growing, which saturates towards $I_{\rm out} \approx 0.9$ as Ω_{s0} is sufficiently large $\Omega_{s0} \gg \Omega_p, \delta$. Actually, the essence of that can also be understood by the properties of dispersion and absorption. From Fig. 4(b) it is observed that the dispersion σ^R_{gm} is critically odd with a big amplitude as $\Omega_{s0} \to 0$, but it becomes nonodd with decreasing amplitude for a larger Ω_{s0}. That is to say, a big modulation by the coupling field will lead to a convergence of the diffraction, but the UD pattern persists due to $\delta \neq 0$. Accordingly, the absorption σ^I_{gm}

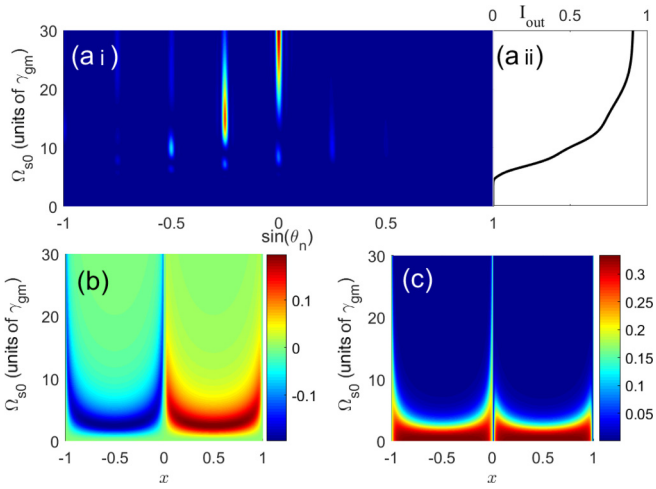

FIG. 4. Same as Fig. 2 except that all physical quantities are shown with respect to Ω_{s0}. Other specific parameters are $\delta = 5.0\gamma_{gm}$ and $\Omega_p = 0.5\gamma_{gm}$.

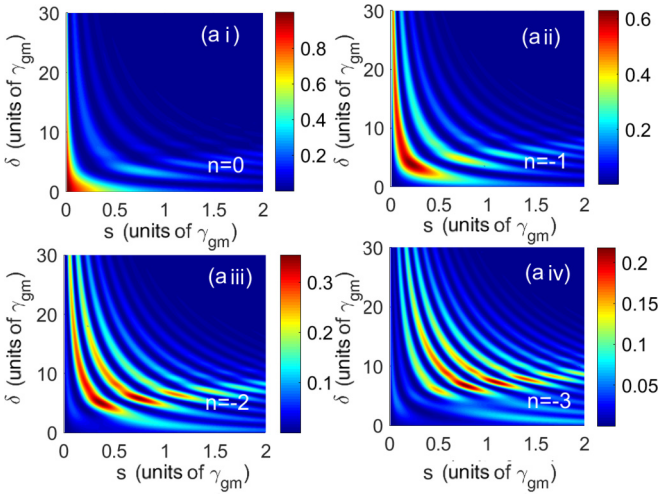

FIG. 6. Maximal diffraction intensity $I_p^{pk}(\theta_n)$ of nth orders versus the vdW interaction s and the modulation amplitude δ for (ai) $n = 0$, (aii) $n = -1$, (aiii) $n = -2$, and (aiv) $n = -3$.

of the medium remains an even function, however with rapidly decreasing amplitude and width as Ω_{s0} increases, perfectly agreeing with the behavior of I_{out}, since a big absorption of medium represents a weak diffraction, and vice versa.

Figure 5 shows specific results of dispersion σ_{gm}^R, absorption σ_{gm}^I, transmission $|T(x)|$, and diffraction pattern $I_p(\theta_n)$. It is observed that, at $\Omega_{s0} = 3.0\gamma_{gm}$, the dispersion and absorption are modulated to be broadened and large, which give rise to poor transmission and diffraction intensity. With increasing Ω_{s0} to $15\gamma_{gm}$, the improvement of transmission significantly enhances the intensity of diffraction, leading to a dominant negative first-order diffraction with its efficiency as high as $\sim$0.6. It is expected that, for $\Omega_{s0} = 30\gamma_{gm}$, the transmission is even larger due to the suppression of absorption, which

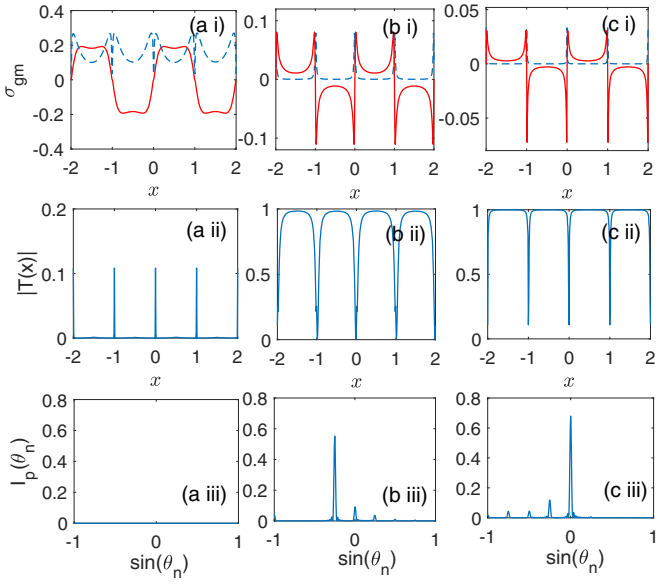

FIG. 5. Parameters σ_{gm}^R, σ_{gm}^I, $|T(x)|$, and $I_p(\theta_n)$ for (a i)–(a iii) $\Omega_{s0}/\gamma_{gm} = 3.0$, (b i)–(b iii) $\Omega_{s0}/\gamma_{gm} = 15$, and (c i)–(c iii) $\Omega_{s0}/\gamma_{gm} = 30$ respectively.

yields a perfect UD with its maximal intensity located in the zeroth-order direction.

By comparing the results from two modulations, we summarize that realizing a perfect UD like the cases of Figs. 3(b iii) and 5(c iii) requires the condition $\Omega_{s0} \gg \delta \gg \Omega_p$. Here the EIG effect with $\Omega_{s0} \gg \Omega_p$ allows a periodic phase and amplitude modulation to the dispersion and absorption of the medium, respectively. In addition, the introduced in-phase modulation for the two-photon detuning serves as a nontrivial control knob that can break the parity of dispersion, leading to unidirectional diffractions. For a perfect UD, its modulation amplitude δ should be moderate.

B. Controllable higher-order diffraction

In a Rydberg EIG, the influence of the vdW shift s directly related to the population of $|r\rangle$ will have a special contribution to the diffraction. Intuitively speaking, s only introduces an energy-level shift due to interactions to the Rydberg state, which is quite different from the role of the position-dependent modulation $\Delta_s(x)$. From its definition [Eq. (10)], it can be seen that an easy way to vary s is by experimentally controlling the average interatomic distance R, allowing the ratio $\xi = (R/R_b)^3$ to vary in a large range. However, we note that the length unit z_0 also depends on ξ, so varying ξ causes a self-consistent change in the interaction length D. To this end, we will study this mutual effect implemented by the vdW interaction s and the interaction length D.

Figures 6(ai)–6(aiv) represent the peak intensity $I_p^{pk}(\theta_n)$ of nth-order diffractions versus s and δ for $n = 0, -1, -2, -3$, respectively. In general, $I_p^{pk}(\theta_n)$ is very sensitive to the values of s and δ, presenting a significant oscillating behavior. Specifically, in the absence of modulation $\delta \to 0$, $I_p^{pk}(\theta_n)$ is expected to continuously decrease with s, satisfying $I_p^{pk}(\theta_0) > I_p^{pk}(\theta_{-1}) > I_p^{pk}(\theta_{-2}) > I_p^{pk}(\theta_{-3})$, as shown in Fig. 7(a i). Similar results have been verified in Ref. [24] as due to the fact that the EIT effect does not work when state $|r\rangle$ is largely shifted, giving rise to a poor higher-order diffraction.

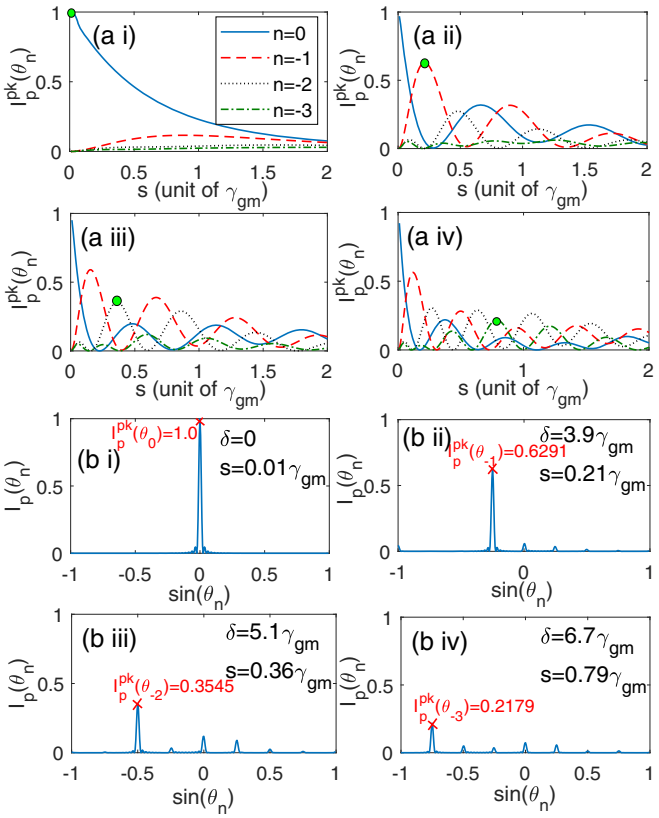

FIG. 7. Peak diffraction intensity $I_p^{\rm pk}(\theta_n)$ versus the vdW interaction s for $n = 0$ (blue solid line), $n = -1$ (red dashed line), $n = -2$ (black dotted line), and $n = -3$ (green dash-dotted line) using (a i) $\delta = 0$, (a ii) $\delta = 3.9\gamma_{gm}$, (a iii) $\delta = 5.1\gamma_{gm}$, and (a iv) $\delta = 6.7\gamma_{gm}$. (b i)–(b iv) Corresponding diffraction patterns $I_p(\theta_n)$ versus $\sin(\theta_n)$ for $n = 0, -1, -2, -3$ with the values of $I_p^{\rm pk}(\theta_n)$, δ, and s given. Here $\Omega_p = 0.5\gamma_{gm}$ and $\Omega_{s0} = 22.5\gamma_{gm}$.

More interestingly, for a nonzero δ, $I_p^{\rm pk}(\theta_n)$ exhibits a rapidly oscillating behavior with the vdW interaction s, which is completely different from the previous finding that the diffraction intensity continuously decreases with s. This significant oscillation with s comes from the mutual effect between s and D because D also increases with s, i.e., ξ^{-1}. Increasing D leads to an enhancement of the dispersion and absorption modulation depth, which further transfers the probe diffraction energy into higher-order directions. For the same reason, by increasing δ, the peak diffraction intensity is also transferred into higher-order directions owing to the enhanced dispersion with δ, as indicated in Fig. 2(b). Therefore, a grating with enhanced higher-order diffraction can be obtained when the values of both δ and s are optimally selected.

Figures 7(a i)–7(a iv) demonstrate the variations of the nth-order peak diffraction intensity versus s for $\delta/\gamma_{gm} = (0, 3.9, 5.1, 6.7)$. It is observed that all nth-order intensities decrease with s for $\delta = 0$. However, once δ is nonzero, the probe diffraction energy continues to transfer into the higher-order directions along the orientation of $I_p^{\rm pk}(\theta_0) \to I_p^{\rm pk}(\theta_{-1}) \to I_p^{\rm pk}(\theta_{-2}) \to I_p^{\rm pk}(\theta_{-3})$ with the enhancement of s, presenting an s-dependent oscillation. Similar oscillations between first- and second-order diffraction intensities with respect to the interaction length was found in Ref. [26].

In Figs. 7(b i)–7(b iv) we show the distributions of the nth-order diffraction intensity by suitably adjusting δ and s, allowing the roles of the zeroth-order, negative first-order, second-order, and third-order diffractions to be dominant, as denoted by green circles in Figs. 7(a i)–7(a iv). By controlling δ and s, we are able to obtain enhanced higher-order diffractions and even the negative third-order diffraction can achieve a maximal diffraction intensity as high as $I_p^{\rm pk}(\theta_{-3}) \approx 0.2179$ when δ and s are enough large to enhance the dispersion.

V. EXPERIMENTAL REALIZATION

Experimental consideration of the implementation of a Rydberg EIG scheme is performed in an ultracold atomic ensemble of ^{87}Rb atoms with energy levels $|g\rangle = 5S_{1/2}|F = 2, m_F = 2\rangle$, $|m\rangle = 5P_{1/2}|F = 3, m_F = 3\rangle$, and $|r\rangle = 62S_{1/2}$. The spontaneous decay of $|m\rangle$ is $\Gamma_e/2\pi = 6.1$ MHz, leading to the dephasing rate $\gamma_{gm}/2\pi = 3.05$ MHz. The dimensionless value η is 7.18×10^{-4} by using $\rho = 5 \times 10^{10}$ cm^{-3}, $\mu_{gm} = 2.534 \times 10^{-29}$ C m, and $\xi = 3.0$, yielding the length unit of the system $z_0 = 1.848$ μm and the optical depth $\zeta = 200$. The resulting interaction length is expected to be $D = 369.6$ μm (equivalent to the values used in, e.g., Ref. [40]), which can be varied in a large range by the average distance R. The probe wavelength is $\lambda_p = 0.25$ μm, by which we can simply assume that the spatial period of the grating is $\Lambda_{sx} = 4\lambda_p = 1.0$ μm. In the simulations we employ a weak probe laser $\Omega_p/2\pi = 1.525$ MHz and a wide-range adjustment for the strong-coupling field $\Omega_{s0}/2\pi \in (0, 91.5]$ MHz in a reasonable range. The auxiliary spatial modulation by Stark shifts from an off-resonant laser field induces a comparable modulation $\Delta_s(x)$ with the amplitude $\delta/2\pi \in (0, 91.5]$ MHz [41]. The typical timescale to reach the steady-state solution is about on the order of microseconds, the same as that used in most experiments. Finally, with an optimum control for parameters we can realize unidirectional higher-order diffractions (see some optimal results summarized in Table I). It is clear that in a strong-blockade environment ($R/R_b < 1$), it is easier to obtain a controlled higher-order diffraction grating with the aid of competitive modulations of δ and Ω_{s0}.

TABLE I. According to Figs. 7(b i)–7(b iv), the optimal values of the peak nth-order diffraction intensity $I_p^{\rm pk}(\theta_n)$ are summarized with the relevant parameters required δ, R/R_b, s, and D. The laser fields are $\Omega_p/2\pi = 1.525$ MHz and $\Omega_{s0}/2\pi = 68.63$ MHz.

Order	Key parameters				Peak intensity
n	δ (MHz)	R/R_b	s (MHz)	D (mm)	$I_p^{\rm pk}(\theta_n)$
0	0	2.73	0.192	0.054	1.0
−1	74.70	0.99	4.022	1.140	0.6291
−2	97.69	0.83	6.895	1.956	0.3545
−3	128.33	0.64	15.132	4.289	0.2179

VI. SUMMARY

We investigated a scheme for realizing an exotic unidirectional Rydberg EIG in a three-level cascade system by implementing a position-dependent two-photon detuning to break the parity of the dispersion of medium. In a normal EIG, the strong SW coupling field introduces a spatially periodic modulation to the refractive index of the medium, which uniformly diffracts the weak TW probe field into positive and negative directions. Here, owing to the parity breaking of dispersion, the transmission function is also affected, leading to a unidirectional diffraction pattern (only the negative-angle direction is diffracted, which depends on the sign of the modulation amplitude δ). We found that it is feasible to design an atomic grating with perfect unidirectional diffractions by using an appropriate modulation amplitude for the two-photon detuning, i.e., $\Omega_{s0} \gg \delta \gg \Omega_p$. Furthermore, differing from the previous result that increasing vdW interaction causes a continuous damping to the nth-order diffraction intensity, here, with the increase of vdW interaction, it has been shown that the maximal nth-order diffraction intensities represent anomalous oscillations and are transferred into higher-order diffractions due to the mutual interplay between the vdW interaction and the interaction length of the medium, which may provide more perspectives from which to realize enhanced higher-order diffractions even in the case of a strong blockade.

Our study offers an approach to improve the intensity of unidirectional higher-order diffraction, providing an opportunity for designing new Rydberg quantum devices such as all-optical quantum switches and large-angle all-optical splitter, based on the technique of Rydberg EIG.

ACKNOWLEDGMENTS

This work was supported by the National Natural Science Foundation of China under Grants No. 11474094, No. 11604086, and No. 11104076, by the Science and Technology Commission of Shanghai Municipality under Grant No. 18ZR1412800, and by the Specialized Research Fund for the Doctoral Program of Higher Education No. 20110076120004.

[1] I. Bloch, J. Dalibard, and W. Zwerger, Many-body physics with ultracold gases, Rev. Mod. Phys. **80**, 885 (2008), and references therein.

[2] H. Briegel, T. Calarco, D. Jaksch, J. Cirac, and P. Zoller, Quantum computing with neutral atoms, J. Mod. Opt. **47**, 415 (2000).

[3] D. Weiss and M. Saffman, Quantum computing with neutral atoms, Phys. Today **70**(7), 44 (2017).

[4] O. Mandel, M. Greiner, A. Widera, T. Rom, T. Hänsch, and I. Bloch, Controlled collisions for multi-particle entanglement of optically trapped atoms, Nature (London) **425**, 937 (2003).

[5] D. Jaksch, J. I. Cirac, P. Zoller, S. L. Rolston, R. Côté, and M. D. Lukin, Fast Quantum Gates for Neutral Atoms, Phys. Rev. Lett. **85**, 2208 (2000).

[6] H. Weimer, M. Müller, I. Lesanovsky, P. Zoller, and H. Büchler, A Rydberg quantum simulator, Nat. Phys. **6**, 382 (2010).

[7] H. Levine, A. Keesling, A. Omran, H. Bernien, S. Schwartz, A. S. Zibrov, M. Endres, M. Greiner, V. Vuletić, and M. D. Lukin, High-fidelity Control and Entanglement of Rydberg-Atom Qubits, Phys. Rev. Lett. **121**, 123603 (2018).

[8] M. Fleischhauer, A. Imamoglu, and J. P. Marangos, Electromagnetically induced transparency: Optics in coherent media, Rev. Mod. Phys. **77**, 633 (2005), and references therein.

[9] O. Firstenberg, C. Adams, and S. Hofferberth, Nonlinear quantum optics mediated by Rydberg interactions, J. Phys. B **49**, 152003 (2016).

[10] J. D. Pritchard, D. Maxwell, A. Gauguet, K. J. Weatherill, M. P. A. Jones, and C. S. Adams, Cooperative Atom-Light Interaction in a Blockaded Rydberg Ensemble, Phys. Rev. Lett. **105**, 193603 (2010).

[11] S. Baur, D. Tiarks, G. Rempe, and S. Dürr, Single-Photon Switch Based on Rydberg Blockade, Phys. Rev. Lett. **112**, 073901 (2014).

[12] C. Murray, A. Gorshkov, and T. Pohl, Many-body decoherence dynamics and optimized operation of a single-photon switch, New J. Phys. **18**, 092001 (2016).

[13] H. Gorniaczyk, C. Tresp, J. Schmidt, H. Fedder, and S. Hofferberth, Single-Photon Transistor Mediated by Interstate Rydberg Interactions, Phys. Rev. Lett. **113**, 053601 (2014).

[14] H. Gorniaczyk, C. Tresp, P. Bienias, A. Mandoki, W. Li, I. Mirgorodskiy, H. P. Büchler, I. Lesanovsky, and S. Hofferberth, Enhancement of Rydberg-mediated single-photon nonlinearities by electrically tuned Förster resonances, Nat. Commun. **7**, 12480 (2016).

[15] H. Y. Ling, Y.-Q. Li, and M. Xiao, Electromagnetically induced grating: Homogeneously broadened medium, Phys. Rev. A **57**, 1338 (1998).

[16] M. Mitsunaga and N. Imoto, Observation of an electromagnetically induced grating in cold sodium atoms, Phys. Rev. A **59**, 4773 (1999).

[17] G. C. Cardoso and J. W. R. Tabosa, Electromagnetically induced gratings in a degenerate open two-level system, Phys. Rev. A **65**, 033803 (2002).

[18] A. Brown and M. Xiao, All-optical switching and routing based on an electromagnetically induced absorption grating, Opt. Lett. **30**, 699 (2005).

[19] B. Dutta and P. Mahapatra, Electromagnetically induced grating in a three-level Λ-type system driven by a strong stranding wave pump and weak probe fields, J. Phys. B **39**, 1145 (2006).

[20] S. A. Carvalho and L. E. E. de Araujo, Electromagnetically induced blazed grating at low light levels, Phys. Rev. A **83**, 053825 (2011).

[21] J. Liu, N. Liu, C. Shan, T. Liu, H. Li, A. Zheng, and X. Xie, Electromagnetically induced grating in a crystal of molecular magnets system, Phys. Lett. A **380**, 2458 (2016).

[22] S.-q. Kuang, C.-s. Jin, and C. Li, Gain-phase grating based on spatial modulation of active Raman gain in cold atoms, Phys. Rev. A **84**, 033831 (2011).

[23] V. G. Arkhipkin and S. A. Myslivets, One- and two-dimensional Raman-induced diffraction gratings in atomic media, Phys. Rev. A **98**, 013838 (2018).

[24] S. Asghar, Ziauddin, S. Qamar, and S. Qamar, Electromagnetically induced grating with Rydberg atoms, Phys. Rev. A **94**, 033823 (2016).

[25] Y. Liu, F. Gao, C. Fan, and J. Wu, Asymmetric light diffraction of an atomic grating with PT symmetry, Opt. Lett. **42**, 4283 (2017).

[26] F. Bozorgzadeh and M. Sahrai, All-optical grating in a $V + \Xi$ configuration using a Rydberg state, Phys. Rev. A **98**, 043822 (2018).

[27] W. R. Anderson, J. R. Veale, and T. F. Gallagher, Resonant Dipole-Dipole Energy Transfer in a Nearly Frozen Rydberg Gas, Phys. Rev. Lett. **80**, 249 (1998).

[28] R. Löw, H. Weimer, J. Nipper, J. Balewski, B. Butscher, H. Büchler, and T. Pfau, An experimental and theoretical guide to strongly interacting Rydberg gases, J. Phys. B **45**, 113001 (2012).

[29] A. Browaeys, D. Barredo, and T. Lahaye, Experimental investigations of dipole-dipole interactions between a few Rydberg atoms, J. Phys. B **49**, 152001 (2016).

[30] L. Béguin, A. Vernier, R. Chicireanu, T. Lahaye, and A. Browaeys, Direct Measurement of the van der Waals Interaction Between Two Rydberg Atoms, Phys. Rev. Lett. **110**, 263201 (2013).

[31] T. E. Lee, H. Häffner, and M. C. Cross, Antiferromagnetic phase transition in a nonequilibrium lattice of Rydberg atoms, Phys. Rev. A **84**, 031402(R) (2011).

[32] J. Sheng, M. Miri, D. Christodoulides, and M. Xiao, PT-symmetric optical potentials in a coherent atomic medium, Phys. Rev. A **88**, 041803(R) (2013).

[33] M. Hning, D. Muth, D. Petrosyan, and M. Fleischhauer, Steady-state crystallization of Rydberg excitations in an optically driven lattice gas, Phys. Rev. A **87**, 023401 (2013).

[34] B. J. DeSalvo, J. A. Aman, C. Gaul, T. Pohl, S. Yoshida, J. Burgdörfer, K. R. A. Hazzard, F. B. Dunning, and T. C. Killian, Rydberg-blockade effects in Autler-Townes spectra of ultracold strontium, Phys. Rev. A **93**, 022709 (2016).

[35] J. Han, T. Vogt, and W. Li, Spectral shift and dephasing of electromagnetically induced transparency in an interacting Rydberg gas, Phys. Rev. A **94**, 043806 (2016).

[36] J. Qian, X.-D. Zhao, L. Zhou, and W. Zhang, Anisotropic deformation of the Rydberg-blockade sphere in few-atom systems, Phys. Rev. A **88**, 033422 (2013).

[37] D. Petrosyan, J. Otterbach, and M. Fleischhauer, Electromagnetically Induced Transparency with Rydberg Atoms, Phys. Rev. Lett. **107**, 213601 (2011).

[38] J.-H. Wu, M. Artoni, and G. C. La Rocca, Non-Hermitian Degeneracies and Unidirectional Reflectionless Atomic Lattices, Phys. Rev. Lett. **113**, 123004 (2014).

[39] G. Alber and W. Strunz, Atom-optical gratings induced by multiphoton excitation of electronic Rydberg wave packets, Phys. Rev. A **50**, 3577(R) (1994).

[40] Y. Liu, X. Tian, X. Wang, D. Yan, and J. Wu, Cooperative nonlinear grating sensitive to light intensity and photon correlation, Opt. Lett. **41**, 408 (2016).

[41] C. Hang, G. Huang, and V. V. Konotop, $\mathcal{PT}$ Symmetry with a System of Three-Level Atoms, Phys. Rev. Lett. **110**, 083604 (2013).